

Manganese cryptomelane-type oxides: A thermo-kinetic and morphological study

J.S. Valente^a, D. Frías^b, P. Navarro^b, M. Montes^b,
J.J. Delgado^d, E. Fregoso-Israel^c, E. Torres-García^{a,*}

^a Instituto Mexicano del Petróleo, Eje Central # 152, 07730 México, D.F., Mexico

^b Applied Chemistry Department, University of the Basque Country (UPV-EHU), Apartado 1072, 20080 San Sebastián, Spain

^c Instituto de Investigación en Materiales, UNAM, México, D.F. 04510, Mexico

^d Departamento de Ciencia de los Materiales e Ingeniería Metalúrgica y Química, Inorgánica de la Universidad de Cádiz, C/ República Saharaui s/n Aptdo. 40, Puerto Real, Cádiz, Spain

Received 5 September 2007; received in revised form 18 October 2007; accepted 18 October 2007

Available online 24 October 2007

Abstract

In the present work, a detailed study on structural and textural properties, as well as a thermo-kinetic characterization of two manganese cryptomelane-type oxides, was carried out. A suitable methodology was stated for determining the several stages taking place during the surface molecules' removal. Thus, further insights were provided about the chemical nature of the sites present at the solid's surface. Relative strengths and the number of basic sites at the surface were estimated. The results show that the removal of the adsorbed (H₂O, CO₂) molecules from the surface is essential to disclose the oxide surface features. The morphological properties and thermo-kinetic characterization indicate the existence of at least three types of basic sites, owing activation energy values ranging from 140 to 190 kJ/mol. The dispersion observed in the activation energy data, during the CO₂ loss, suggests that the interaction occurs on different sites. Therefore, both samples showed a heterogeneous surface; this is related to the energetic nature of the sites, as well as the basic strengths of the surface manganese cryptomelane oxides.

© 2007 Elsevier B.V. All rights reserved.

PACS : 68.35.-p; 68.47.Gh; 81.70.Pg

Keywords: Manganese cryptomelane oxides; Hi-Res TGA; Kinetics in solid; Thermal analysis; Isoconversion method

1. Introduction

Transition metal oxides, such as molybdenum, tungsten, vanadium, and manganese oxides with different oxidation states, supported or not, are one of the most studied systems because of their wide range of applicability in oxidation reactions, especially in the hydrocarbon oxidation process [1–6]. The oxidation process can be considered an effective way of reducing the emission of an important class of air pollutants emitted from many industrial processes. Surprisingly, nearly all these reactions, whether they have high or significant selectivity, proceed over a small number of high-valence metal oxides.

The use of manganese cryptomelane-type oxides has attracted considerable attention in the last years. These compounds

represent a good alternative to decrease the use of noble metals in many heterogeneous catalytic processes, particularly in the oxidation process, such as CO reduction automotive emission [6,7]. The manganese cryptomelane-type oxides are tunnel structured compounds based on MnO₆ octahedra, which create channels of different sizes, depending on the combination of octahedral structures; hence, they allow the preparation of solids with several stoichiometric compositions [5,6].

In this work, we are focused on the thermo-kinetic behavior of two manganese cryptomelane-type oxides obtained under different preparation methods. Cryptomelane oxides are an important family, often used as a model structure, since many oxides can be prepared in a wide variety of oxidation states, for instance, the preparation of MMnO_x solids with different compositions, in the presence of alkaline or alkaline-earth cations (M). Accordingly, the study of the solids, synthesized here, is interesting because the physico-chemical properties of the manganese cryptomelane-type oxides are likely influenced by the preparation method.

* Corresponding author. Tel.: +52 55 91758430; fax: +52 55 91758429.

E-mail address: etorresg@imp.mx (E. Torres-García).

2. Materials and methods

2.1. Preparation of cryptomelane oxides

Two samples were prepared as follows: the first sample, a cryptomelane oxide denoted as PAM, was prepared by using the process reported by [8]. A solid–solid mixture of KMnO_4 and $\text{Mn}(\text{CH}_3\text{COO})_2$, in the absence of solvents, was prepared by mixing weighted amounts of both solids (0.06 mol KMnO_4 and 0.09 mol $\text{Mn}(\text{CH}_3\text{COO})_2$), guaranteeing a stoichiometric ratio of 2/3. The solid mixture was milled for 1 h and afterwards placed in a sealed plastic container at 80 °C for 4 h. The resulting solid was washed repeatedly with deionized water until the elimination of ions was complete. Finally, the solid was dried at 80 °C for 12 h, following calcination at 10 °C/min up to 450 °C and was maintained at this temperature for 2 h.

The second sample, a cryptomelane oxide denominated AM, was prepared by the reflux method following the procedure reported by Luo et al. [2]. Eleven grams of $\text{Mn}(\text{CH}_3\text{COO})_2$ in 40 ml deionized distilled water (DDW) was dissolved in a buffer solution consisting of 5 ml of glacial acetic acid and 5 g of $\text{K}(\text{CH}_3\text{CO}_2)$ in 40 ml DDW. Separately, 6.5 g of KMnO_4 were dissolved in 150 ml of DDW and then slowly added to the refluxed solution and kept under stirring and reflux for 24 h. Afterwards, the resulting suspension was separated by filtration, washed with distilled water, and dried at 120 °C for 24 h. The resulting powder was calcined at 450 °C for 2 h.

2.2. X-ray diffraction

The solid samples were examined by X-ray diffraction (XRD) using a Phillips PW 1729-1820 diffractometer using $\text{Cu K}\alpha$ radiation. Phase identification based on XRD patterns was assisted by the ICDD-PDF-2 database.

2.3. Electron microscopies (TEM and SEM)

Samples were analyzed through transmission electron microscopy (TEM) in a JEOL 200 Kv JEM-2200FS. Calcined samples (at 450 °C/2 h) were dispersed in ethanol before placing them on the copper grid with Formvar support. Scanning electron microscopy (SEM) analysis was carried out with a Hitachi S-2700 scanning electronic microscope (voltage 15 kV). Prior to analysis, the samples were covered with gold and mounted over a carbon film.

2.4. Textural analysis

The texture of the calcined samples (at 450 °C/2 h) was analyzed by N_2 adsorption–desorption isotherms at –196 °C on a Micromeritics ASAP 2020 apparatus. Prior to the analysis, the samples were outgassed in a vacuum (10^{-5} Torr) at 300 °C for 4 h. The surface areas were calculated by using the Brunauer–Emmett–Teller (BET) method, and the pore size distribution and total pore volume were determined by the Brunauer–Joyner–Hallenda (BJH) method.

2.5. Temperature-programmed desorptions (TPD-MS)

The evolution of the thermal desorption products was followed in an AUTOSORB-1 apparatus coupled with a PRISMA-QMS 200 quadrupole spectrometer.

A sample of ~100 mg was heated from room temperature to 500 °C at a rate of 10 °C/min under N_2 flow rate of 100 ml/min. The samples were not submitted to any special pretreatment. The gaseous products were monitored by simultaneously measuring the mass/charge signals 18, 32, and 44, corresponding to H_2O , O_2 , and CO_2 , respectively. For the purpose of adjusting the detection parameters to each sample, prior to the test, a scan was carried out on every sample to identify the species emitted.

2.6. Thermal analysis

A TA Instrument's high resolution (Hi-ResTM) thermogravimetric analyzer TGA 2950, and the instrument control software Thermal Advantage version 1.1A, were used to obtain the weight loss profile of the samples studied. The TGA 2950 was used in dynamic rate mode. In this mode, the heating rate is varied dynamically during the heating ramp in response to the derivative of weight change (as derivative increases, the heating rate is decreased and vice versa). The heating rates were constrained to the range from 0.001 °C/min up to the maxima: 5, 10, 20, and 50 °C/min with samples' weight of about 10 mg in all cases and instrumental resolution of 5. The sensitivity of the balance was 10^{-7} g and the furnace was purged with a nitrogen flow of 100 ml/min.

The temperature modulated differential scanning calorimetry (TMDSC) data were obtained with a DSC (TA Instruments, MDSC–2910 model), from an initial temperature of –20 °C (stabilized over 5 min), to a final temperature of 500 °C, a modulation of ± 0.318 °C each 60 s and a ramp of 2 °C/min under N_2 atmosphere, and hermetic pans. The samples' weight was approximately 5 mg in all cases. The TMDSC technique provides the changes in total heat flow during the process, which represents only heat flow measured by conventional DSC that, in this case, is separated into two components. One component is a function of the samples' heat capacity and heating rate (C_p, β), “reversing heat flow,” and the other one is a function of absolute temperature and time [$f(T,t)$], “non-reversing heat flow.” The non-reversing component of the total heat is determined as the arithmetic difference between the total heat and the heat capacity component [9]. Total heat flow and its reversible and non-reversible fractions during the study of any process are powerful tools for understanding the nature of the thermal process involved in the sample [10–12].

3. Results and discussion

3.1. Structural characterization

XRD patterns obtained from the samples are presented in Fig. 1. All possible reflections of cryptomelane compounds (JCPDS 29-1020) are present with characteristic reflections

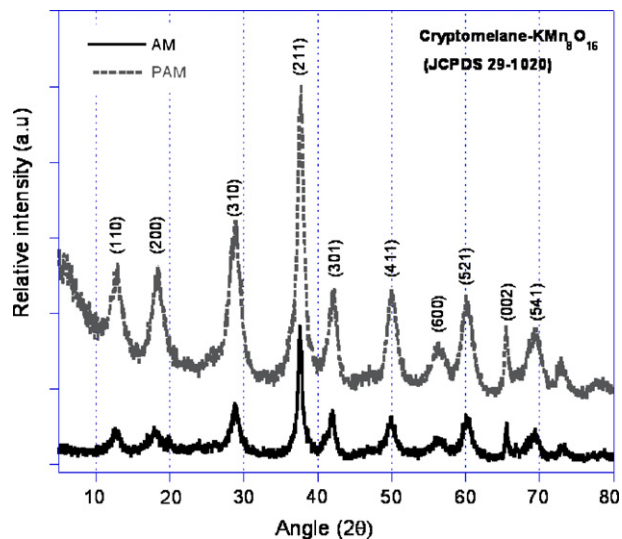


Fig. 1. XRD patterns of the samples prepared by solid–solid mixture (PAM) and reflux method (AM).

(angle position $2\theta = 12.8^\circ, 18.5^\circ, 28.9^\circ, 37.5^\circ, 42^\circ,$ and 50°). According to Fig. 1, the microcrystalline solids obtained show a monophasic cryptomelane-type structure. Apart from the width and relative intensities of the different peaks associated with the cryptomelane phase, no substantial differences were detected as a function of the preparation procedure; such that, from X-ray pattern observations, we can only suggest that AM cryptomelane shows higher crystallinity than PAM. From a structural point of

view, this analysis indicates that the preparation procedures (reflux and solid–solid milled) used in each case mainly affect the solid's crystallinity. It is worthwhile to note, however, that control of the solid's crystallinity is an important parameter, since it can be related to the morphological and textural properties of the material, and thus with its catalytic performance.

3.2. Morphological analysis

The transmission electron micrograph shows that the samples were made up of regularly shaped platelet-like units (see top images in Fig. 2A and B). Even if a similar morphology had been observed in both samples, the AM platelets were larger and more organized than those observed in the PAM material, indicating a better crystallization in the former. This result is in agreement with the crystallinity observed in the AM sample by means of the XRD technique. In fact, the SEM analysis of AM (see left bottom image of Fig. 2C) revealed that the sample was made up of bundles of fibers with sizes ranging from 2 to 5 μm , whilst PAM consisted of rounded aggregates with average sizes smaller than 0.5 μm (see right bottom image of Fig. 2D). The morphology of the samples agrees well with that already reported in the literature [13]. The SEM micrographs show that the morphology of the samples is quite different and this variation was surely a consequence of the preparation methods used in each case.

The adsorption–desorption isotherms of the calcined samples showed that both are of type IV, which characterizes

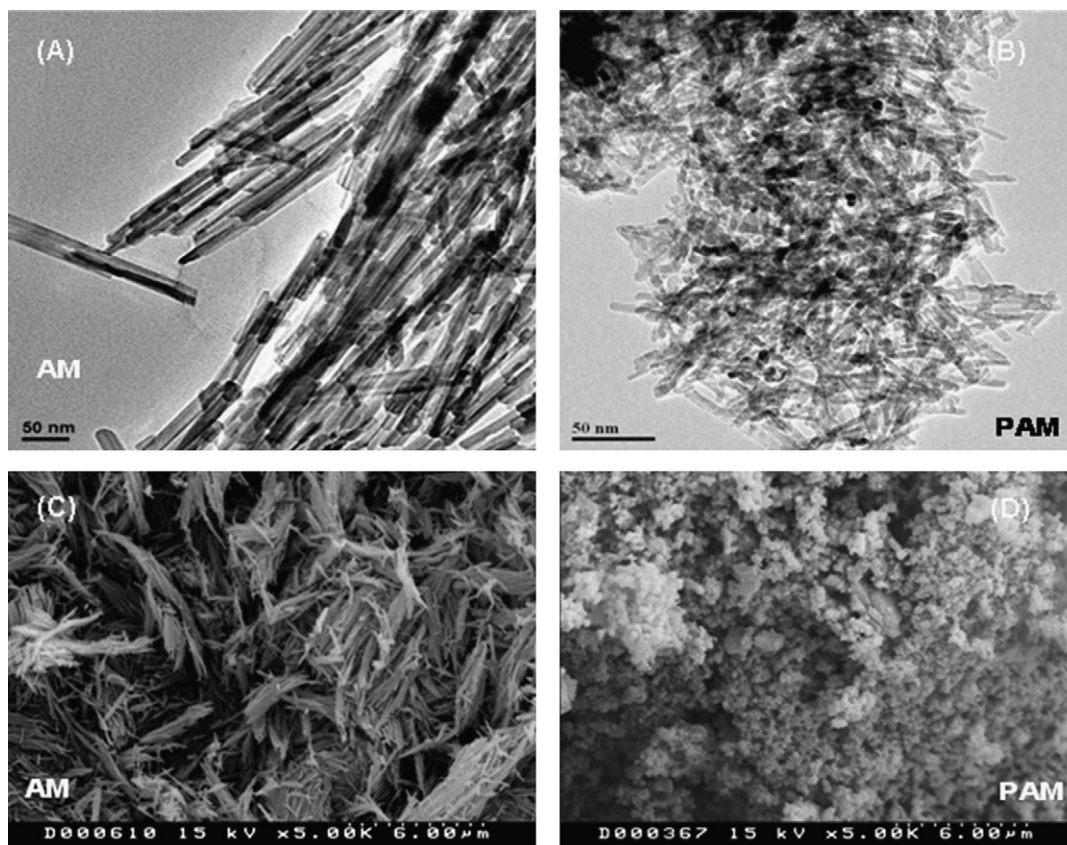


Fig. 2. A and B: TEM (top images) and C and D: SEM (bottom images) analysis over the AM and PAM samples.

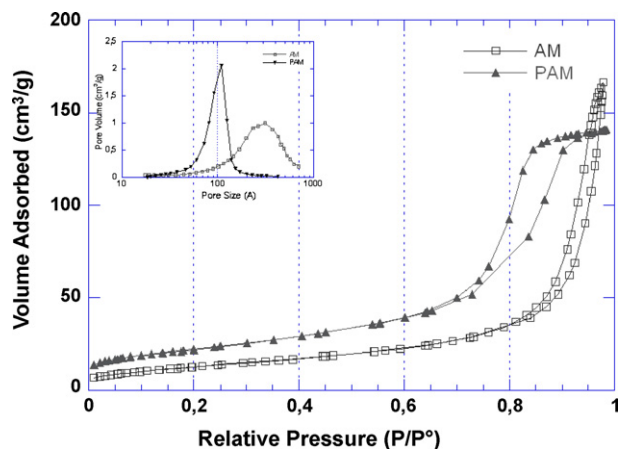


Fig. 3. N₂ Adsorption–desorption isotherms of samples calcined at 450 °C/2 h: (▲) PAM and (□) AM. Inset shows corresponding pore size distributions.

mesoporous solids, as shown in Fig. 3. A multilayer nitrogen adsorption process takes place from the beginning due to the low relative pressure (P/P^0) where the adsorption start indicates the weak adsorption enthalpy of adsorbate–adsorbent. However, the PAM sample clearly showed a divergence in its adsorption path, presenting its inflection point at approximately $P/P^0 = 0.70$, while that in the AM sample was continuous until $P/P^0 = 0.85$ (see Fig. 3). Taking into account that the adsorption process is intimately related to the solid's morphology [14], it is obvious that morphological variations of the solids, due to their preparation method, must be appreciated here. This difference could be understood by analyzing the hysteresis loops, since they manifest a capillary condensation of adsorbate in the mesopores of solids. According to IUPAC classification, the hysteresis loop for the AM sample is type H3 [14], which is in agreement with the morphology observed by SEM on this material, usually given by adsorbents containing slit-shaped pores [14]. The H2 type hysteresis loop of the PAM sample, comprised between $0.70 < P/P^0 < 0.90$, is typically found on solids with homogeneous pore distribution; therefore, this sample evidences a more regular geometry than that noticed in AM, as shown in the Fig. 3 inset, where a narrow pore size distribution was observed in PAM. The AM sample showed a heterogeneous pore size distribution; see the corresponding inset in Fig. 3.

It is well known that the range of the specific surface area can vary widely depending upon the particle size and shape and also the porosity. The relationship between surface area (S_p), the total pore volume (V_p) and the average pore radius (r_p) is given by:

$$S_p = f \times \frac{V_p}{r_p} \quad (1)$$

where f depends upon the pore geometry [15]. In Table 1 we reported the specific surface areas, pore volume, and average pore size of the calcined solids. The pore size was strongly related to the solid's crystallite size: large crystallites produced large pores (Table 1 and inset of Fig. 3). Also, when r_p increases

Table 1
Textural Properties of calcined solids at 450 °C/2 h

Sample	BET surface area S_p (m ² /g)	Pore volume V_p (cm ³ /g)	Average pore diameter (r_p) (nm)
AM	107	0.55	30
PAM	177	0.49	11

and V_p remains almost constant, the S_p decreases considerably from 177 to 107 m²/g; see PAM and AM values.

In summary, the PAM sample showed the higher specific surface area with a narrow pore size distribution, in addition to a pore volume value nearer to that of AM (Table 1). Thus, the morphological and textural properties of the cryptomelane-type oxides could be controlled by the method employed to prepare them.

3.3. Temperature-programmed desorption (TPD-MS) results

TPD-MS curves were used to obtain information on the thermal profile and evolution of main species, such as H₂O, O₂, and CO₂. It has been observed (Fig. 4a and b) that at least four thermal events are clearly defined during the thermal desorption process and that the main species are H₂O and CO₂. Meanwhile, it is important to note that the desorption of O₂ does not pass through a maximum, presenting a constant value throughout the entire thermal study, which suggests that the oxygen is not desorbed, at least up to 500 °C. Additionally, these results indicate that the samples spontaneously adsorb carbon dioxide and water from the air at room temperature.

According to the TPD-MS data, the water releases are characterized by events at 188 and 320 °C for AM and 202 and 304 °C for PAM. By contrast, the CO₂ evolution curve as a function of temperature can be divided into at least three stages related to its interaction with the surface of the oxides. The first two effects, at about 215–225 °C and 280 °C, are overlapped with a water release process, probably due to the existence of hydrogen-carbonate species formed by the interaction of CO₂ with basic OH groups.

It is interesting to note that the most important events are present ca. at 280 °C and 370–380 °C for both samples; these zones are related to a high release of CO₂, observed in the TPD-MS curves. The presence of these events at different temperatures suggests that the CO₂ molecules are linked to the surface in a different form. Furthermore, the thermal stability of the CO₂ molecules is surely related to the heterogeneity of the basic sites.

According to the TPD-MS curves, the thermal profile of the CO₂ molecule release occurs in a similar temperature range for both samples; however, their signal intensity from the third effect is markedly different (see Fig. 4). Taking into account that the intensity is related to the basic site's number, hence the AM has stronger basic sites than the PAM, this result suggests that the variability in intensity and magnitude during the CO₂ molecule release at about 370–380 °C is the consequence of a complex combination of structural defect density and chemical nature.

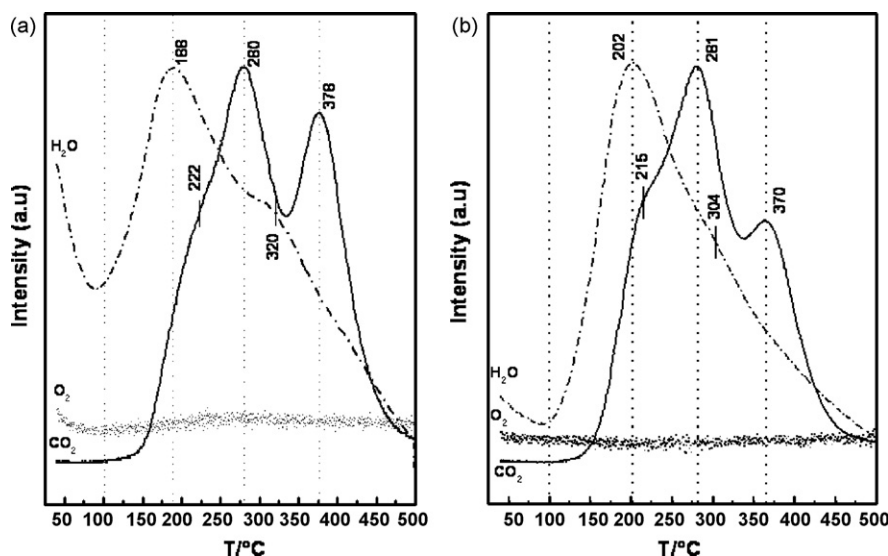


Fig. 4. TPD-MS profiles of $m/e = 18, 32,$ and 44 (H_2O , O_2 and CO_2 , respectively) during the thermal treatment in N_2 of: (a) AM and (b) PAM.

3.4. High resolution TGA analysis

Hi-Res TGA curves were used to obtain information on the amount and nature of the components in the residual solid, such as water and carbon dioxide, as well as to find the dependence of $(E)_\alpha$ with α for the different stages observed in the weight loss versus T -curves.

The typical thermal profiles of the AM and PAM samples, obtained by Hi-Res TGA, are shown in Fig. 5A and B. In general, four main thermal events can be distinguished up to 400°C . The samples lose mass continuously between room temperature and 350°C . The total weight loss, up to 350°C ,

relative to the initial weight was 3.8 wt.% for AM and 6.8 wt.% for PAM. The initial weight loss, below 100°C , is associated with the release of weakly bonded water molecules (physical water). The main and second weight loss, observed in both compounds between 90 and 235°C , which can be divided into at least two thermal events, is assigned to the water + carbon dioxide release. The simultaneous releases of $(\text{H}_2\text{O} + \text{CO}_2)$ during these stages, detected in our TPD-MS studies, revealed the complexity of this process and suggest the presence of hydrogen-carbonate species. Additionally, a small loss of mass occurring between 230 and 330°C is also related to the removal of more carbon dioxide, which can be tentatively assigned to

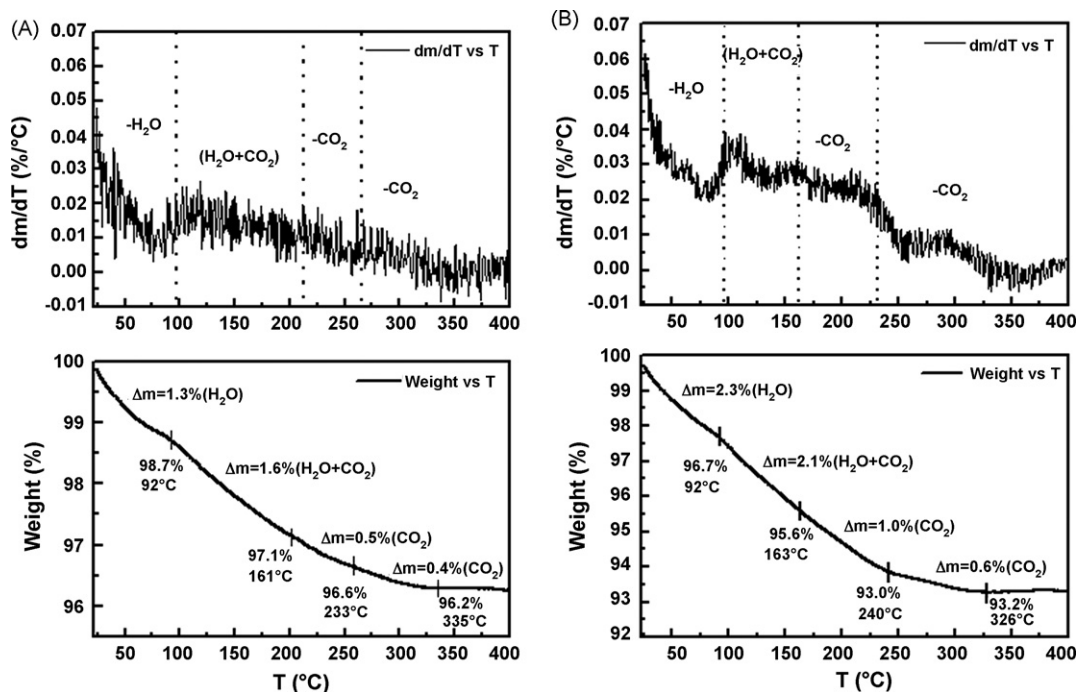


Fig. 5. Typical thermal profile for manganese cryptomelane-type oxides: (a) AM and (b) PAM samples, obtained via Hi-Res TGA. For these cases the heating rates were constrained between 0.001 and $5^\circ\text{C}/\text{min}$.

bidentate carbonate species absorbed, in agreement with the TPD-MS results [16].

As the temperature increases, we can see that the molecules covering the surface are successively desorbed according to their interaction strength with the surface sites. Thus, the molecules weakly associated with the surface are desorbed at lower temperatures (i.e., physical water), and those that interact strongly are desorbed at higher temperatures (i.e., surface ^-OH groups and/or hydrogen-carbonate species, unidentate and bidentate carbonate). These results point out that the variability in magnitude and position of these events may be related to the chemical nature of sites, as well as the number and distribution of the surface sites, which are closely related to the textural properties and crystal structures of the oxide.

From a chemical point of view, the results suggest the existence of several $Mn^{n+}-O-Mn^{m+}$ ion pairs of different coordination numbers (i.e., unsaturated metal sites) as well as some oxygen coordination sites that function as Lewis basic sites, (surface O^{2-} anions). Consequently, different sites are generated as the activation temperature increases. The basic sites generated by removing the molecules covering the surface were unveiled by the detection of acidic species such as H_2O and CO_2 .

In spite of this, it is difficult to determine strength on a finite scale and calculate the sites quantitatively. Relative strengths and number of sites, on the different catalysts, can be estimated by carrying out the Hi-Res TGA experiments under similar conditions.

Our hypothesis is that the density of sites per square nanometer can be estimated from the relationships between Hi-Res TGA curves, textural properties and adequate chemical criterion. According to this, if weight losses between 90 and 235 °C, and up to 350 °C correspond to the removal of three types of chemical species, we can estimate that the weight losses of each stage can be associated quantitatively with number of sites on surface.

Thus, assuming these criteria, the weight losses of 1.6 and 2.1 wt.% for AM and PAM, respectively, could be assigned to hydrogen-carbonate species ($-HCO_3$) release, which corresponds to 1.4 and 1.2 sites per nm^2 , in each case. Considering that by each $-HCO_3$ species released, two types of surface OH groups (i.e., a basic OH and an acid OH group) are necessary to generate two surface center basic O^{2-} ions (see schematic representation in Fig. 6, site I), this corresponds finally to a total of 2.8 and 2.4 basic sites per nm^2 , respectively.

The second weight losses of 0.5 wt.% for AM and 1.8 wt.% for PAM, observed between 160 and 235 °C, are related with

unidentate carbonate species, formed by interaction with surface basic oxygen centers in the form of O^{2-} ions (see Fig. 6, site II), and correspond to 0.6 and 1.4 sites per nm^2 , respectively.

Finally, during the last stage, weight losses of 0.4 and 0.6 wt.%, between 230 and 340 °C, in both samples, are assigned to bidentate carbon dioxide desorption, corresponding to the formation of 0.5 surface sites per nm^2 , in either sample. This results indicate that during the bidentate carbon dioxide release, two different sites are generated, a basic site, associated with surface O^{2-} ions; and two center acid sites, related to the formation of unsaturated metal Mn^{n+} , Mn^{m+} sites. This certainly is not a massive modification of the oxide's structure, at least up to 350 °C, and indeed corresponds to the formation essentially of basic sites by releasing H_2O and CO_2 molecules from the surface. Thus, the PAM solid should have approximately 10% more basic sites than AM.

Up to this point, our results suggest that the presence of surface basic sites, whether in mutual cooperation or not, for a specific catalytic reaction, is an important factor when tailoring the match between the reaction and chemical affinity. Therefore, it is necessary to establish an adequate balance between the chemical nature of the sites, the relative strength and the number of basic sites at the surface, depending on the mechanistic aspects of the catalyzed chemical reaction. A schematic representation of the three above mentioned surface sites can be found in Fig. 6.

3.5. Modulated differential scanning calorimetry (MDSC) study

From temperature modulated differential scanning calorimetric (TMDSC) curves in the region between -20 and 500 °C (Fig. 7A and B), the presence of various endothermic events can be observed as a common characteristic in the samples. These events are associated with the enthalpies (adsorption's heats) of different processes that are surely related to the release of H_2O and CO_2 molecules. The endothermic peaks around 100 °C for both samples correspond to the same thermal effect detected by Hi-Res TGA between room temperature and 90 °C: the release of physical water. In both samples, the total heat flow associated with the dehydration is dominated by the non-reversible component ($\Delta H_{global} = 118$ J/g vs. $\Delta H_{irrev} = 106$ J/g for AM and $\Delta H_{global} = 114$ J/g vs. $\Delta H_{irrev} = 109$ J/g for PAM, respectively), which indicates that this thermal effect is essentially an irreversible process, within the time scale of this experiment.

Once the physical water molecules have evolved, at least four endothermic processes are detected in the TMDSC curves (Fig. 7A and B). This fact could be related to a variation in the composition of residual oxide, associated essentially with a different process of bicarbonate, unidentate carbonate and bidentate carbonate desorption during heating. An important observation is that the total heat flow is dominated by the irreversible component (*function of absolute temperature and time* [$f(T,t)$]). This could be interpreted as a kinetic effect: the modulation time for the DSC heating ramp turns out to be insufficient in allowing the re-adsorption of a large fraction of the removed surface species.

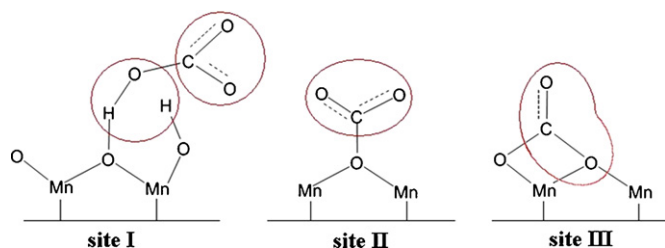


Fig. 6. Schematic representation of three probable surface types sites.

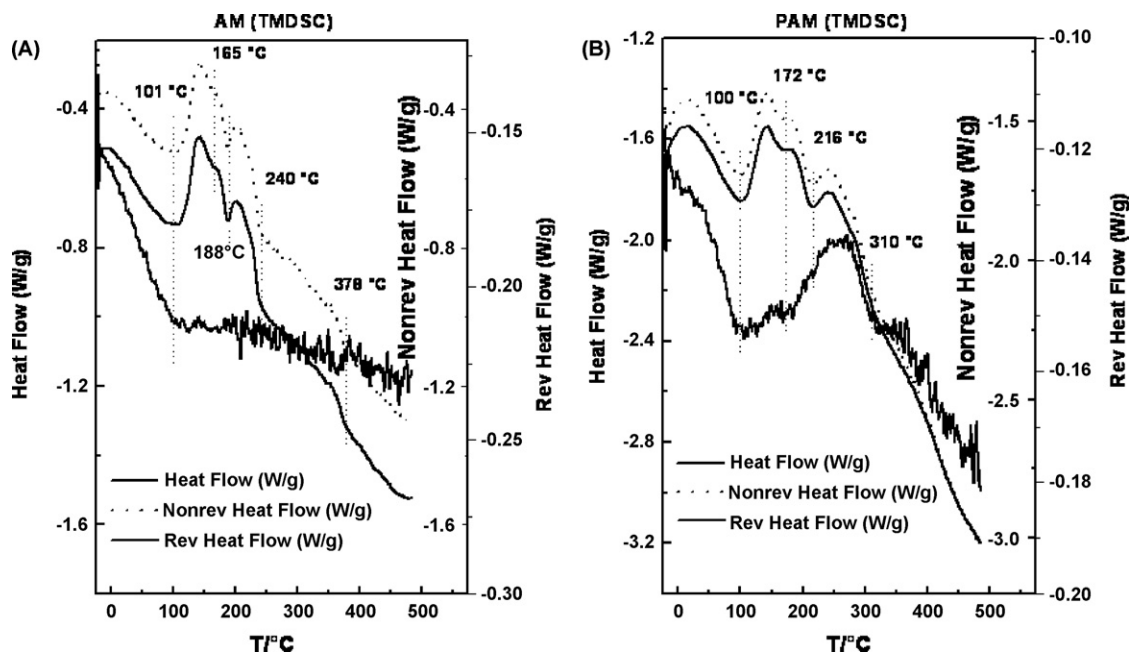


Fig. 7. Thermal profile obtained by temperature modulated differential scanning calorimetry (TMDSC) for: (a) AM and (b) PAM samples.

On the other hand, the observed changes in the base line from room temperature for the reversible heat curve are attributed to variations in the sample heat capacity due to the composition changes promoted by the release of H_2O and CO_2 . Furthermore, rearrangement of surface atoms, during thermal treatment, cannot be discarded, in addition to the molecules' desorption.

4. Kinetic study

Finally, the experimental Hi-Res TGA data were processed using the isoconversion principle in order to obtain the dependence of the activation energy (E_α) as a function of the transformation degree α of the solid. This methodology has been described previously [17–19]. It states that the rate at constant extent of conversion is only a function of the temperature, and that $f(\alpha)$ is independent of the heating rate. If the Arrhenius equation is applicable, we can write:

$$\left[\frac{d \ln(d\alpha/dt)}{dT^{-1}} \right]_\alpha = -\frac{E_\alpha}{R} \quad (2)$$

where the subscript α indicates the values of isoconversion, $(\alpha_i)_1 = (\alpha_i)_2 = \dots (\alpha_i)_n$, for each experiment and temperature. This criterion allows an estimation of (E_α) without the assumption of any reaction model, i.e., the model-free method.

The results obtained for different heating rates using Hi-Res TGA and applying Eq. (2) are shown in Fig. 8. The profile for these curves (Fig. 8) shows the different changes undergone by the (E_α) as a function of α . These results show a complex (E_α) on α dependence and reveal the typical energetic behavior of the different surface sites during molecule release. The activation energy data presents variations, between 140 and 190 kJ/mol for all reaction ranges. In general, three possible

zones with slope changes of about $\alpha = 0.35$ and 0.65 were detected. Therefore, the existence of these zones is a clear indication of the different chemical nature of the surface sites and suggests that the H_2O and CO_2 molecules are linked to the surface in a different form.

At the beginning of the thermal desorption process (zone I) between 0.1 and 0.35 of conversion, the activation energy values are substantially different in both samples (see Fig. 8).

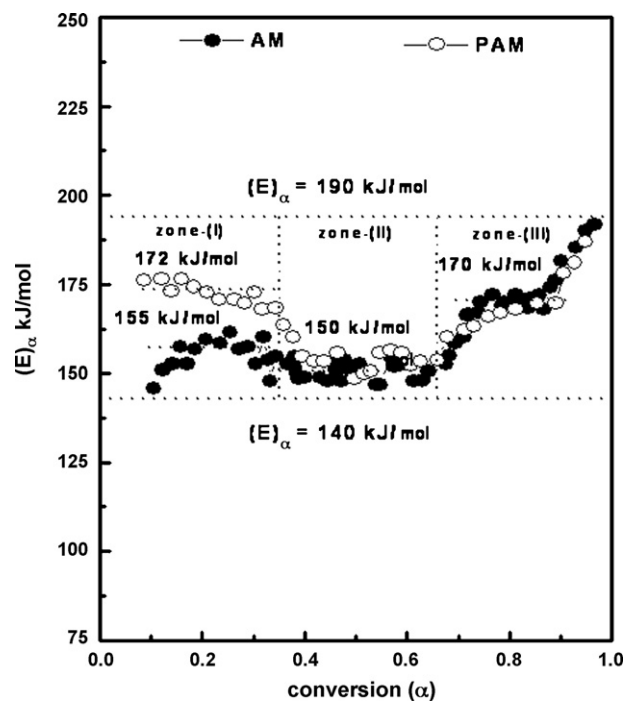


Fig. 8. Dependence of the (E_α) as a function of the transformation degree (α), determined by the isoconversion method during the release of CO_2 molecules between 80 and 330 °C in AM and PAM samples.

This fact might be associated with the surface basic site's difference in strengths for this temperature range, related to the presence of hydrogen-carbonate species, formed by the interaction of CO₂ with surface basic OH groups. At $\alpha > 0.30$ (zone II), the dependence decreases to about 150 kJ/mol, and $(E)_\alpha$ is essentially constant as α changes from 0.35 to 0.65. This suggests that the nature of the desorption sites, during this stage, are energetically equivalent in both samples, which are likely related to the existence of unidentate carbonate formed by interaction with surface basic oxygen centers in the form of O²⁻ ions. Finally, for the last stage (zone III), in the range $0.70 \leq \alpha \leq 0.98$, the activation energy increases from 150 kJ/mol up to a constant value of about 170 kJ/mol, then rises up to reach 190 kJ/mol near the end of the desorption process. This stage is associated with the presence of strong basic sites, which are tentatively assigned to bidentate carbonate species on surface. This consideration clearly suggests that not only O²⁻ basic sites but also adjacent metallic sites participate in CO₂ adsorption [20].

Unfortunately, energetic differences during the CO₂ release (zones II and III), between both samples as a function of the transformation degree (α), are not significant, and we can only suggest that these sites are energetically equivalent. In addition to the above mentioned, the variations in the $(E)_\alpha$ slopes can be related with changes in the reaction mechanism, associated with the chemical nature of surface interaction.

Finally, it is interesting to note that the magnitude of the activation energy values between 140 and 190 kJ/mol clearly suggests that the H₂O and CO₂ molecules are linked to the surface by means of a chemical bond. Therefore, these results provide additional confirmation concerning the relative strengths of the basic surface sites.

5. Conclusions

These results show the influence of the preparation method on the physico-chemical nature of the manganese cryptomelane oxides studied, particularly on textural properties.

The correlation of textural properties and thermo-kinetic characterization allowed the relative estimation of the surface sites and clearly indicates the existence of at least three site types in both oxides.

The dispersion of the activation energy values between 140 and 190 kJ/mol during H₂O and CO₂ release suggests that the interaction occurs on different surface sites, indicating the heterogeneous surface character and the energetic nature

of the sites. Moreover, the presence of acidic molecules such as H₂O and CO₂ on the surface indicates the surface character of basic sites.

The variability in position and magnitude of the thermal events, as well as the relative abundance of these sites, may be related to the chemical nature, number, and distribution of the surface sites, which are closely related to the textural properties and crystal structures of the oxide. This can be understood by assuming that the relative abundance of these sites widely depends upon the particle size and shape.

From a structural point of view, the presence of different site types can be associated with: (i) the presence of basic centers (surface O²⁻ anions and/or -OH groups) and (ii) the existence of ion pairs with low coordination numbers, which can exist at corners, edges, or high Miller index surface planes.

References

- [1] F.M. Bautista, J.M. Campelo, D. Luna, J. Luque, J.M. Marinas, *Appl. Catal. A* 325 (2007) 336.
- [2] J. Luo, Q. Zhang, A. Huang, S.L. Suib, *Micropor. Mesopor. Mater.* 35–36 (2000) 209.
- [3] B.M. Weckhuysen, D.E. Keller, *Catal. Today* 78 (2003) 25.
- [4] M.R. Morales, B.P. Barbero, L.E. Cadús, *Appl. Catal. B* 67 (2006) 229.
- [5] R. Jothiralingam, B. Viswanathan, T.K. Varadarajan, *J. Mol. Catal. A* 252 (2006) 49.
- [6] W. Gac, *Appl. Catal. B* 75 (2007) 107.
- [7] Y.F. Shen, R.P. Zerger, R.N. DeGuzman, S.L. Suib, L. McCurdy, D.I. Potter, C.L. O'Young, *Science* 260 (1993) 511.
- [8] Y.-S. Ding, X.-F. Shen, S. Sithambaram, S. Gomez, R. Kumar, V.M.B. Crisostomo, S.L. Suib, M. Aindow, *Chem. Mater.* 17 (2005) 5382.
- [9] R.L. Danley, *Thermochim. Acta* 402 (2003) 91.
- [10] A. Valor, S. Kycia, E. Torres-García, E. Reguera, C. Vázquez-Ramos, F. Sánchez-Sinencio, *J. Solid State Chem.* 172 (2003) 471.
- [11] E. Torres-García, A. Peláiz-Barranco, C. Vázquez-Ramos, G.A. Fuentes, *J. Mater. Res.* 16 (8) (2001) 2209.
- [12] E. Torres-García, J. Balmaseda, L.F. del Castillo, E. Reguera, *J. Therm. Anal. Cal.* 86 (2) (2006) 371.
- [13] D.M. Frias, S. Nouisir, I. Barrio, M. Montes, L.M. Martínez, T.M.A. Centeno, J.A. Odriozola, *Appl. Catal. A* 325 (2007) 205.
- [14] F. Rouquerol, J. Rouquerol, K. Sing, *Adsorption by Powder & Porous Solids*, Academic Press, New York, 1999.
- [15] A. Lecloux, *Comptes-rendus de la semaine d'étude de la catalyse*, Université de Liège Ed., vol. 64, 1970, p. 169.
- [16] H. Hattori, *Chem. Rev.* 95 (1995) 537.
- [17] S. Vyazovkin, C.A. Wigh, *Annu. Rev. Phys. Chem.* 48 (1997) 125.
- [18] S. Vyazovkin, *Thermochim. Acta* 355 (2000) 155.
- [19] G. Rodríguez-Gattorno, L.F. del Castillo, E. Torres-García, *Thermochim. Acta* 435 (2005) 176.
- [20] F. Can, A. Travert, V. Ruaux, J.-P. Gilson, F. Maugé, R. Hu, R.F. Wormsbecher, *J. Catal.* 249 (2007) 79.